Frequency Acquisition and Tracking in High Dynamic Environments

Yu T. Su and Ru-Chwen Wu

***Abstract*—This paper presents mean squared error (MSE) analysis of two classes of frequency acquisition and tracking algorithms. Additive white Gaussian noise as well as Rician fading channels are considered. The class of batch-processing algorithms is an extension of earlier least squares proposals used in more benign (lower dynamic) environments. These algorithms try to fit the phase trajectory of the down-converted samples of a received signal. Such a trajectory will depend on the histories of both the signal and the local frequency variations when the local frequency is updated recursively. We propose a method to solve this difficulty and present both first-order and second-order recursive algorithms. Numerical results demonstrate that the MSE performance predicted by our analysis is consistent with that estimated by computer simulation and that the proposed algorithms not only provide rapid acquisition times but also give small tracking jitters.**

***Index Terms*—Frequency synchronization, least squares estimation, satellite communication.**

I. Introduction

CARRIER recovery is an important issue in designing a communication system. The fact that the relative movement between the transmitter and the receiver induces various degrees of frequency variation at the receiving end makes it even more critical in a mobile communication channel. This problem is especially difficult to overcome in a high dynamic environment such as mobile low-earth-orbit (LEO) satellite communications. To illustrate this point, let us consider a continuous-wave (CW) signal $s(t) = \cos \omega t$ transmitted from a radio source. The time delay Δt between the transmitter and the receiver can be evaluated by $\Delta t = r(t - \Delta t)/c \approx r(t)/c$, where c is the speed of light and $r(t)$ is the slant distance between the transmitter and the receiver at time t. The received signal $y(t)$ can thus be expressed as

$$\begin{aligned} y(t) &= As(t - \Delta t) = A \cos[\omega(t - \Delta t)] \\ &= A \cos[\theta(t)] \approx A \cos[\omega(t - r(t)/c)]. \end{aligned} \tag{1}$$

Manuscript received October 3, 1998; revised March 15, 2000. This work was supported in part by the National Science Council, Taiwan, R.O.C., under Grant NSC 82-0401-F-002-004. Parts of this paper were presented at the 1993 International Symposium on Communications, Hsinchu, Taiwan, and at VTC'97, Phoenix, AZ.

Y. T. Su is with the Department of Communication Engineering and the Microelectronics and Information Systems Research Center, National Chiao Tung University, Hsinchu, Taiwan (e-mail: ytsu@cc.nctu.edu.tw).

R.-C. Wu is with the Computer Communication Laboratory, Industrial Technology Research Institute, Hsinchu, Taiwan.

Publisher Item Identifier S 0018-9545(00)09187-8.

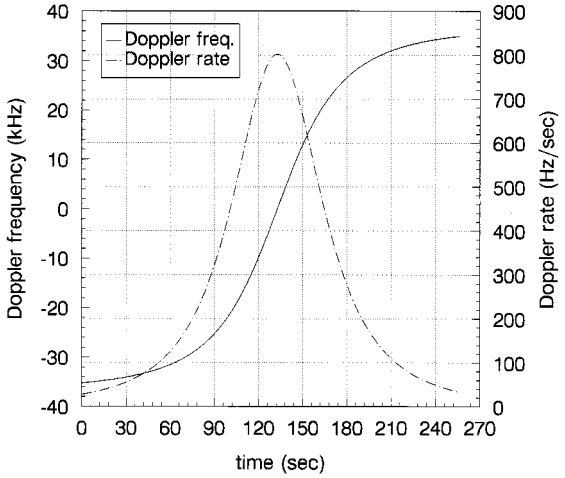

Fig. 1. Doppler frequency and Doppler rate at ground terminal for a 1.5-GHz signal transmitted from a LEO satellite with 350-km altitude.

Assuming the existence of various order of derivatives, we have

$$\begin{aligned} r(t) = {} & r(t - \Delta t) + \dot{r}(t - \Delta t)\Delta t \\ & + \frac{1}{2!}\ddot{r}(t - \Delta t)(\Delta t)^2 + \cdots . \end{aligned} \tag{2}$$

Equations (1) and (2) imply that the total phase $\theta(t)$ of the received signal is given by

$$\begin{aligned} \theta(t) = \omega t - \frac{\omega}{c}\Big[& r(t - \Delta t) + \dot{r}(t - \Delta t)\Delta t \\ & + \frac{1}{2!}\ddot{r}(t - \Delta t)(\Delta t)^2 + \cdots \Big]. \end{aligned} \tag{3}$$

Define the equivalent baseband signal's phase as $\tilde{\theta}(t) = \theta(t) - \omega t$. The first and second derivatives of $\tilde{\theta}(t)$, denoted by $\omega_D(t)$ and $\dot{\omega}_D(t)$, are known as the Doppler frequency and Doppler rate (or differential Doppler), respectively. Fig. 1 depicts the Doppler and Doppler rate, seen by an earth terminal, of a 1.5-GHz signal that is transmitted from a LEO satellite traveling in circular earth orbit with an altitude $h = 350$ km. The time span of approximately 270 s represents the time elapsed for the satellite to travel from 20° to 160° of elevation angle. For this particular case, the Doppler frequency and Doppler rate can be as high as 35 kHz and 800 Hz/s, respectively.

Coherent phase-shift keying such as binary phase-shift keying (BPSK) and quadrature phase-shift keying (QPSK) are the most popular modulation schemes employed in digital satellite communication links. But these modulations are not very tolerant of link disturbances like high Doppler rates, specular multipath, and

ionospheric anomalies. To combat large Doppler and differential Doppler uncertainties, the Costas carrier tracking loop used to demodulate QPSK signals must have a relatively wide bandwidth, and this will cause a significant threshold degradation. Thus, a Costas loop or other phase-locked loops for coherent reception may require frequency acquisition aids in a high dynamic environment. Automatic frequency control (AFC) [1], [2] loops are often employed to serve such a need. However, an AFC loop may not be capable of meeting the fast acquisition/reacquisition specification commonly required in large Doppler uncertainty or high dynamic condition. Some modifications of conventional AFC loops have been proposed [6]; although these schemes result in performance improvement, they are quite computationally demanding.

On the other hand, (3) implies that the baseband signal phase can be expressed as

$$\tilde{\theta}(t+\Delta t) = \tilde{\theta}(t) + \omega_D(t)\Delta t + \frac{\dot{\omega}_D(t)}{2!}(\Delta t)^2 + R(t,\,\Delta t) \quad (4)$$

where the remainder $R(t,\,\Delta t)$ is $O[(\Delta t)^3]$ as $\Delta t \to 0$. This fact suggests that a second-order polynomial (in Δt) approximation of the received baseband phase within a short time period can in fact provide estimators for the Doppler frequency and the differential Doppler. In other words, given the phase samples $\tilde{\theta}(1), \tilde{\theta}(2), \ldots, \tilde{\theta}(N)$, obtained at $t_1, t_2, \ldots, t_N$ ($t_1 < t_2 < \cdots < t_N$), respectively, we want to find $(\hat{\theta}_0, \hat{\omega}_D, \hat{\dot{\omega}}_D)$ such that

$$e(N) = \sum_{i=1}^{N}[\tilde{\theta}(i) - \hat{\theta}(i)]^2, \quad (5a)$$

$$\hat{\theta}(i) = \hat{\theta}_0 + \hat{\omega}_D\Delta t_i + \frac{1}{2!}\hat{\dot{\omega}}_D(\Delta t_i)^2, \quad \Delta t_i = t_i - t_0 \quad (5b)$$

is minimized, t_0 being the initial observation time. The solution is well known

$$\hat{\dot{\omega}}_D = 2\alpha_N/T_S^2\sum_{k=1}^{N}\tilde{\theta}(k)\left[k^2 - (N+1)k + \frac{\gamma_N}{6}\right] \quad (6)$$

$$\hat{\omega}_D = \alpha_N/T_S\sum_{k=1}^{N}\tilde{\theta}(k) \cdot \left[\frac{\beta_N}{15}k - \frac{(2N+1)\gamma_N}{10} - (N+1)k^2\right] \quad (7)$$

where $\alpha_N = 180/[N(N+1)(N-1)(N+2)(N-2)]$, $\beta_N = (2N+1)(8N+11)$, $\gamma_N = (N+1)(N+2)$.

If a first-order least squares (LS) fit is used, we will obtain an estimate for the Doppler frequency only. The first-order solution is given by

$$\hat{\theta}_0 = \frac{2\sum_{k=1}^{N}(2N+1-3k)\tilde{\theta}(k)}{N(N-1)} \quad (8)$$

$$\hat{\omega}_D = \lambda_N\sum_{k=1}^{N}(2k-N-1)\tilde{\theta}(k) \quad (9)$$

where $\lambda_N = (6/T_S N(N+1)(N-1))$.

Su [3], Tretter [5], and Bellini *et al.* [4] proposed a first-order LS method to estimate a fixed frequency offset. Chuang [11] used a similar approach for burst-mode frequency recovery. Knowles and Waltman [17] and Lang and Musicus [16] used the second-order solution, assuming fixed frequency and frequency rate offsets. Kumar [12], [13] applied LS estimation to various series expansions of the received signal. Some other algorithms based on signal phase or frequency samples were derived [14]–[17]. Most of these algorithms are one-shot, batch form schemes that offer estimate(s) for a fixed frequency offset (and/or frequency rate). Some of them are capable of tracking a slow-varying frequency [1], [2], [6], [10], [13]. In applications where computational simplicity is required, the fixed-gain $\alpha\beta$ filter may be used [18]. However, it is suitable for small dynamic conditions only. The well-known maximum likelihood (ML) principle can be applied to estimate frequency offset [7]–[10]. But ML methods cannot necessarily provide a fast estimate unless the candidate frequency uncertain range is very limited.

This paper presents two classes of frequency acquisition and tracking algorithms. The first class provides frequency update information for the local numerical-controlled oscillator (NCO) every T_F seconds, while the second class continuously offers such support. These algorithms not only can deal with a large frequency variation range but also yield rapid acquisition time and small steady-state jitter. The ensuing section describes both classes of algorithms, considers the phase reconstruction problem, and discusses the data modulation issue. Section III presents the mean squared prediction error analysis. Unlike previous presentations, we do not assume a Gaussian distribution for the phase reconstruction error. Simulation results that validate our proposals and analysis are shown in Section IV. The last section summarizes our major results.

II. Frequency Acquisition and Tracking Algorithms

A. Phase Recovery and Data Modulation Issues

To implement our algorithms, the baseband phase information $\tilde{\theta}(t)$ has to be extracted from the received waveform first. When the only perturbation is additive white Gaussian noise (AWGN), the optimal phase estimator is known to be given by $\hat{\theta}(k) = \tan^{-1}[Q(k)/I(k)]$, where $I(k)$ and $Q(k)$ are the in-phase and quadrature-phase components of the baseband signal sampled at $t_k = kT_S$, for $k = 1, 2, \ldots, N$, i.e.,

$$I(k) = A\cos[\tilde{\theta}(t_k)] + n_I(k) \quad (10a)$$

$$Q(k) = A\sin[\tilde{\theta}(t_k)] + n_Q(k) \quad (10b)$$

where T_S is the sampling period and $n_I(k)$, $n_Q(k)$ are independent and identically distributed (i.i.d.) Gaussian random variables with the common variance σ_n^2. However, such a phase estimator can only render relative phase information (module 2π). To derive the absolute phase that reflects the true phase variation history, we need a different phase reconstruction method. This can be accomplished if we keep track of the phase difference $\Delta\theta(k)$ between two adjacent samples. The absolute phase

can then be obtained by accumulating phase differences sequentially, while the latter is to be derived from

$$\Delta\hat{\theta}(k) = \cos^{-1} \cdot \left[\frac{I(k)I(k-1) + Q(k)Q(k-1)}{\sqrt{I^2(k) + Q^2(k)}\sqrt{I^2(k-1) + Q^2(k-1)}} \right]. \tag{11}$$

The sign of the phase difference (increasing or decreasing) is determined by the locations of the two consecutive sample pairs $\{I(k-1), Q(k-1)\}$ and $\{I(k), Q(k)\}$, assuming that the sampling rate is fast enough to ensure that they are less than 180° apart. As long as this assumption is valid, phase differences can be obtained by table lookup using ROM.

Although our algorithms are based on an unmodulated carrier assumption, they can be modified for some digital modulated signals. Bellini *et al.* [4] suggested that a fourth-power law device be used to remove the data modulation of a QPSK signal. We can also fit the reconstructed phases $\{2\tilde{\theta}(k)\}$ of a received BPSK sequence or, equivalently, let the signal sequence pass through the concatenation of a square-law device and a low-pass filter. Both operations remove BPSK modulation at the expense of incurring a so-called squaring loss, which is an increasing function of the data bandwidth. The above methods are special cases of a general approach for removing PSK data modulation via memoryless nonlinear processing [19].

Other approaches include decision-directed processing algorithms that utilize a detected data sequence [20]–[23] or data-aided processing algorithms that invoke a known data pattern [23]–[25]. Nevertheless, all these methods assume that the symbol timing is known and can be categorized as timing-directed approaches. This assumption is not very realistic during the acquisition mode but is valid for the tracking mode. When symbol timing information is not available and/or frequency uncertainty is large, one of the other more complicated phase recovery (unwrapping) algorithms [3], [26]–[28] that require higher sampling rates is needed. Unfortunately, at low carrier-to-noise ratio (CNR), the reliability of these algorithms becomes doubtful.

Hence, it is safe to say that our algorithms need either an unmodulated preamble or a memoryless nonlinearity preprocessor for acquisition purpose. They can be used in conjunction with one of the timing-directed phase unwrapping methods (data-aided, decision-directed) to deal with the modulated carrier case during the tracking mode.

B. Batch Form Algorithms

We first consider a simple extension of the LS approach for use in frequency tracking. We notice that a first-order LS solution (8), (9), even in the absence of noise, still suffers from estimation error caused by truncating the higher order (second-order and up) terms of the Taylor series (3). In general, for an $(n-1)$th-order approximation over the time period $[t_1, t_2 = t_1 + \Delta t]$, the truncation error (remainder term) is bounded by

$$|R_n(t, \Delta t)| \le \frac{\omega}{c} \frac{|\Delta t|^n}{n!} \sup_{t_1 \le t \le t_2} \left| \frac{d^n r(t)}{dt^n} \right|. \tag{12}$$

Since the second-order term is not often negligibly small, as Fig. 1 has shown, this kind of modeling error alone can thus make a first-order estimate unreliable. Moreover, in a dynamic environment where the received carrier frequency is not a constant, an estimate for the differential Doppler is needed not only for a more reliable estimation but also for the prediction of the future frequency variation, as the Taylor series expansion for $\omega_D(t)$

$$\omega_D(t + \Delta t) = \omega_D(t) + \dot{\omega}_D(t)\Delta t + \cdots \tag{13}$$

tells us that the estimators, $\hat{\omega}_D(t)$ and $\hat{\dot{\omega}}_D(t)$, can be used to produce an accurate prediction for $\omega_D(t + \Delta t)$ if Δt is small.

Using the LS estimation and prediction solutions, we can easily form a batch-processing periodically updated frequency acquisition/tracking algorithm as follows.

1) Reconstruct N consecutive baseband phases by

$$\tilde{\theta}(k) = \sum_{i=1}^{k} \Delta\hat{\theta}(i) \tag{14}$$

where $\Delta\hat{\theta}(i)$ is the ith recovered signal phase difference. The set $\{\tilde{\theta}(k), k = 1, 2, \ldots\}$ will be referred to as the reconstructed or the compensated phase trajectory.

2) Estimate the Doppler (and Doppler rate) by using (9) or (6) and (7) to fit the reconstructed phases in the least squares sense.
3) Feed the above estimator(s) to the NCO to update the frequency of the local signal. The updated frequency (and frequency rate) is used until next estimator(s) is obtained T_F seconds later.

For the first-order algorithm, the updated frequency is equal to the sum of the current frequency plus the newly estimated frequency offset. The second-order algorithm uses (13) to update the local frequency every Δt seconds. The new estimator(s) $\hat{\omega}_D$ ($\hat{\dot{\omega}}_D$) will be used until the next estimation is obtained T_F seconds later, T_F being the update period; see Fig. 2. The second step can be generalized to an mth-order LS estimation algorithm, i.e., fitting the reconstructed baseband phase trajectory by an mth-order polynomial

$$\hat{\theta}(t) = \hat{\theta}_0 + \hat{\omega}_D t + \frac{1}{2!}\hat{\dot{\omega}}_D t^2 + \frac{1}{3!}\hat{\ddot{\omega}}_D t^3 + \cdots + \frac{1}{m!}\hat{\omega}_D^{(m-1)} t^m \tag{15}$$

for $0 \le t \le NT_S$. Here we are interested in the least squares solution $\{\hat{\omega}_D, \hat{\dot{\omega}}_D, \ldots, \hat{\omega}_D^{(m-1)}\}$, instead of the real phase of received signal. The choice of the order m, as will become clear in Section III, depends on the desired mean squared error (MSE) performance, the sampling rate, the channel dynamic, and the channel noise statistic.

C. Recursive Algorithms

The error associated with the above tracking algorithms comes from three different sources. The first one is the baseband phase reconstruction process, (11) and (14), the second one arises from using only finite terms of the Taylor series (4) to model the received signal's phase, and the third one has to

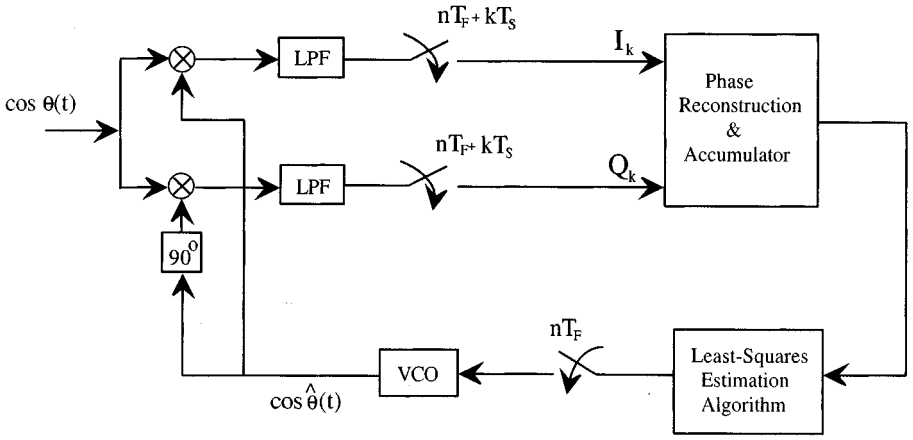

Fig. 2. Block diagram of the proposed LS frequency acquisition and tracking system.

do with the frequency predictor that uses a truncated version of (13). They are referred to as the phase reconstruction error, modeling error, and truncation error, respectively. As will be shown in the next section, the MSE of the above LS algorithm is a function of these three errors and the sample size (N) used.

For a batch-processing algorithm, the predictors are used to control the NCO output frequency before the next set of predictors is obtained T_F seconds later, the MSE right after a set of new predictors is obtained is dominated by the phase reconstruction error. As time elapses, the modeling and truncation errors will increase. The specification of T_F depends mainly on the maximum modeling and truncation errors we can tolerate. Decreasing the update period T_F can reduce these two errors at the expense of a perhaps larger estimation (Doppler or Doppler rate) error due to a smaller sample size. The benefit of using a recursive algorithm is thus obvious: one can reduce the modeling and truncation errors to a minimum while keep the sample size fixed.

To have an efficient implementation of such a real-time algorithm, we would like the estimators be computed recursively. In other words, after using the set $\{\tilde{\theta}(k),\, k = 1, 2, \ldots, N\}$ to derive the estimator(s) and update the NCO frequency, we input the new phase sample $\tilde{\theta}(N+1)$, and then, based on $\{\tilde{\theta}(k),\, k = 2, 3, \ldots, N+1\}$, compute our new estimator(s). Conceptually, the algorithm works as if we have applied a sliding window of size N to the reconstructed phase trajectory so that estimators are continuously derived from the member samples within the window. Like a batch-processing algorithm, a basic assumption of such an algorithm is that the N consecutive phase samples within a window are functions of the received frequency and noise only. This assumption is no longer valid for a recursive implementation since the reconstructed phase trajectory, $\{\tilde{\theta}(k),\, k = 1, 2, \ldots\}$, with $T_F = T_S$, has been "compensated" by the local frequency source due to the feedback by our predictors. More specifically, for the batch-processing algorithm, the phase samples in the same batch result from mixing with the same local NCO frequency, while for a candidate recursive algorithm, every reconstructed phase sample is produced by mixing the received I, Q samples with distinct local frequencies. Therefore, to implement the recursive algorithm, we have to recover the uncompensated phase trajectory. This can be realized by using a "bookkeeping" register, which keeps track of the accumulated compensations and the restored original uncompensated phase trajectory [see (a.4) and (b.6) in Table I(a) and (b), where $\tilde{\theta}$ and θ represent the compensated and uncompensated phases, respectively, and $\tilde{\theta}(k) = \theta(k)$ for $k = 1, 2, \ldots, N$]. Using this idea, we can then remove the effect of the local frequency variation from the down-converted sample phases. After some algebraic manipulations, we obtain the first-order and second-order algorithms listed in Table I(a) and (b), respectively. The first-order algorithm requires seven additions and five multiplications per iteration, while the second-order algorithm requires 15 additions and 12 multiplications per iteration. Note that the recursive algorithm presented in [16] does not update the frequency whenever a new sample is obtained. The purpose of that algorithm is to derive a pair of unknown but fixed frequency and frequency rates; therefore it does not have to deal with the difficulty we meet here.

III. Mean Squared Frequency Error Analysis

We will denote $\epsilon_{r_i}(k)$ as the difference between the true phase and the reconstructed phase of the ith-order algorithm at $t = t_k$, $\epsilon_{m_i}(k)$, and ϵ_{tr_i}, the corresponding phase model error, and the truncation error associated with the frequency predictor, respectively.

To have a prediction of the frequency offset at $t_f (> t_{N+1})$, we can use either $\hat{\omega}_D(t_f) = \hat{\omega}_D(t_0) + \hat{\dot{\omega}}_D(t_0)(t_f - t_0)$ or $\hat{\omega}_D(t_f) = \hat{\omega}_D(t_{N+1}) + \hat{\dot{\omega}}_D(t_{N+1})(t_f - t_{N+1})$. Because both pairs of estimators, $\{\hat{\omega}_D(t_0), \hat{\dot{\omega}}_D(t_0)\}$ and $\{\hat{\omega}_D(t_{N+1}), \hat{\dot{\omega}}_D(t_{N+1})\}$, are based on the same set of samples, they should have the same phase reconstruction error, but the other two kinds of error can be different. For the first-order LS algorithm, the phase model error and the resulting MS estimation errors of $\hat{\omega}_D(t_0)$ and $\hat{\omega}_D(t_{N+1})$ are the same. But the consideration of the frequency prediction error favors the choice of the latter predictor because it results in a smaller maximum truncation error; see (12). Expressing the true frequency at time $t = t_f$ as

$$\begin{aligned}\omega_D(t_f) &= \omega_D(t_{N+1}) + \dot{\omega}_D(t_{N+1})\Delta t + \cdots \\ &= \omega_D(t_{N+1}) + \epsilon_{tr_1}, \end{aligned} \tag{16}$$

TABLE I
(a) SUMMARY OF THE FIRST-ORDER RECURSIVE FREQUENCY ACQUISITION AND TRACKING ALGORITHM. (b) SUMMARY OF THE SECOND-ORDER RECURSIVE FREQUENCY ACQUISITION AND TRACKING ALGORITHM

Initialization:

$a_0(1) = \sum_{k=1}^{N} \theta(k)$ (a.1)

$a_1(1) = \sum_{k=1}^{N} k\theta(k)$ (a.2)

$\hat{\omega}_D(1) = \lambda_N[2a_1(1) - (N+1)a_0(1)]$ (a.3)

Recursive estimation: at each sampling instant, $n = 2, 3, \cdots$ compute

$\theta(n+N-1) = \tilde{\theta}(n+N-1) + \hat{\omega}_D(n-1)T_S - \theta(n)$ (a.4)

$\Delta a_1(n) = N\theta(n+N-1) - a_0(n-1)$ (a.5)

$\Delta a_0(n) = \theta(n+N-1) - \theta(n-1)$ (a.6)

$\Delta\hat{\omega}_D = \lambda_N[2\Delta a_1(n) - (N+1)\Delta a_0(n)]$ (a.7)

$a_0(n) = a_0(n-1) + \Delta a_0(n)$ (a.8)

$\hat{\omega}_D(n) = \hat{\omega}_D(n-1) + \Delta\hat{\omega}_D(n)$ (a.9)

(a)

Initialization:

$a_0(1) = \sum_{k=1}^{N} \theta(k)$ (b.1)

$a_1(1) = \sum_{k=1}^{N} k\theta(k)$ (b.2)

$a_2(1) = \sum_{k=1}^{N} k^2\theta(k)$ (b.3)

$\hat{\omega}_D(1) = \alpha_N/T_S[-(N+1)\Delta a_2(1) + \frac{\beta_N}{15}\Delta a_1(1) - \frac{(2N+1)\gamma_N}{10}\Delta a_0(1)\Big]$ (b.4)

$\hat{\omega}_D(1) = 2\alpha_N/T_S^2[\Delta a_2(1) - (N+1)\Delta a_1(1) + \frac{\gamma_N}{6}\Delta a_0(1)]$ (b.5)

Recursive estimation: at each sampling instant, $n = 2, 3, \cdots$ compute

$\theta(n+N-1) = \tilde{\theta}(n+N-1) + \hat{\omega}_D(n-1)T_S - \theta(n)$ (b.6)

$\Delta a_2(n) = N^2\theta(n+N-1) + a_0(n-1) - 2a_1(n-1)$ (b.7)

$\Delta a_1(n) = N\theta(n+N-1) - a_0(n-1)$ (b.8)

$\Delta a_0(n) = \theta(n+N-1) - \theta(n-1)$ (b.9)

$\Delta\hat{\omega}_D(n) = \alpha_N/T_S[-(N+1)\Delta a_2(n) + \frac{\beta_N}{15}\Delta a_1(n) - \frac{(2N+1)\gamma_N}{10}\Delta a_0(n)\Big]$ (b.10)

$a_0(n) = a_0(n-1) + \Delta a_0(n)$ (b.11)

$a_1(n) = a_1(n-1) + \Delta a_1(n)$ (b.12)

$\hat{\omega}_D(n) = 2\alpha_N/T_S^2[\Delta a_2(n) - (N+1)\Delta a_1(n) + \frac{\gamma_N}{6}\Delta a_0(n)]$ (b.13)

$\hat{\omega}_D(n) = \hat{\omega}_D(n-1) + \Delta\hat{\omega}_D(n) + \hat{\omega}_D(n)NT_S$ (b.14)

(b)

and the reconstructed phase $\tilde{\theta}(k)$ in (9) as[1]

$$\tilde{\theta}(k) = \omega_D(t_{N+1})(t_k - t_{N+1}) + \epsilon_{m_1}(k) + \epsilon_{r_1}(k) \tag{17}$$

we can calculate the MSE for the first-order Doppler predictor

$$\begin{aligned} &E[(\omega_D(t_f) - \hat{\omega}_D(t_f))^2] \\ &\quad\equiv \sigma^2_{\Delta\omega} \\ &\quad= \frac{12\sigma^2_{\epsilon_{r_1}}}{T_S^2N(N-1)(N+1)} \\ &\qquad+ \left(\epsilon_{tr_1} - \lambda_N\sum_{k=1}^{N}(2k-N-1)\epsilon_{m_1}(k)\right)^2 \end{aligned} \tag{18}$$

[1]This results from the assumption that we always use the normalization $\tilde{\theta}(0) = 0$ or $\tilde{\theta}(N+1) = 0$.

where $\sigma^2_{\epsilon_{r_1}} = E[\epsilon^2_{r_1}(k)]$. If higher order truncation errors can be neglected, i.e.,

$$\begin{aligned} \epsilon_{tr_1} &= \dot{\omega}_D(t_{N+1})(t_f - t_{N+1}) + \cdots \\ &\approx \dot{\omega}_D(t_{N+1})(t_f - t_{N+1}) \end{aligned} \tag{19a}$$

$$\begin{aligned} \epsilon_{m_1}(k) &= \tfrac{1}{2}\dot{\omega}_D(t_{N+1})(t_k - t_{N+1})^2 + \cdots \\ &\approx \tfrac{1}{2}\dot{\omega}_D(t_{N+1})(t_k - t_{N+1})^2 \end{aligned} \tag{19b}$$

the MSE can be approximated by

$$\begin{aligned} \sigma^2_{\Delta\omega} \approx{}& \frac{12\sigma^2_{\epsilon_{r_1}}}{T_S^2N(N-1)(N+1)} + \dot{\omega}_D^2(t_{N+1}) \\ &\cdot[(t_f - t_{N+1}) - T_S(N+1)/2]^2. \end{aligned} \tag{20}$$

For the second-order algorithm, the true frequency at time $t = t_f$ is

$$\omega_D(t_f) = \omega_D(t_{N+1}) + \dot{\omega}_D(t_{N+1})(t_f - t_{N+1}) + \epsilon_{tr_2} \tag{21}$$

and the reconstructed phase $\tilde{\theta}(k)$ derived from (11) and (14) is

$$\begin{aligned} \tilde{\theta}(k) = {}& \tfrac{1}{2}\ddot{\omega}_D(t_{N+1})(t_k - t_{N+1})^2 + \omega_D(t_{N+1})(t_k - t_{N+1}) \\ &+ \epsilon_{m_2}(k) + \epsilon_{r_2}(k). \end{aligned} \tag{22}$$

Hence the MSE for the Doppler predictor becomes

$$\begin{aligned} &E[(\omega_D(t_f) - \hat{\omega}_D(t_f))^2] \\ &\quad= \frac{\alpha_N\sigma^2_{\epsilon_{r_2}}}{180T_S^2}[12(2N+1)(8N+11) + 720/T_S^2 \\ &\qquad\cdot(t_f - t_{N+1})^2 + 720(N+1)/T_S(t_f - t_{N+1})] \\ &\qquad+ \Bigg\{\epsilon_{tr_2} - \frac{\alpha_N}{T_S}\sum_{k=1}^{N}\Bigg[\frac{\beta_N}{15}(k-N-1) + \frac{(2N+1)\gamma_N}{10} \\ &\qquad\qquad+ (N+1)(k-N-1)^2\Bigg] \\ &\qquad\cdot\epsilon_{m_2}(k) - \frac{2\alpha_N}{T_S^2}(t_f - t_{N+1})\sum_{k=1}^{N}[k^2 - (N+1)k + \gamma_N/6] \\ &\qquad\cdot\epsilon_{m_2}(k)\Bigg\}^2. \end{aligned} \tag{23}$$

Similarly, with the approximations of the truncation and the model errors

$$\begin{aligned} \epsilon_{tr_2} &\approx \tfrac{1}{2}\ddot{\omega}_D(t_{N+1})(t_f - t_{N+1})^2 \\ \epsilon_{m_2}(k) &\approx \tfrac{1}{6}\ddot{\omega}_D(t_{N+1})(t_k - t_{N+1})^3 \end{aligned} \tag{24}$$

we have

$$\begin{aligned} \sigma^2_{\Delta\omega} \approx{}& \frac{\alpha_N\sigma^2_{\epsilon_{r_2}}}{180T_S^2}\Bigg[12(2N+1)(8N+11) + \frac{720}{T_S^2} \\ &\cdot(t_f - t_{N+1})^2 + \frac{720(N+1)}{T_S}(t_f - t_{N+1})\Bigg] \\ &+ \ddot{\omega}_D(t_{N+1})\Bigg[\frac{1}{2}(t_f - t_{N+1})^2 + \frac{6N^2+15N+11}{60}T_S^2 \\ &+ \frac{N+1}{2}T_S(t_f - t_{N+1})\Bigg]^2. \end{aligned} \tag{25}$$

The MSE for the Doppler rate estimator or predictor can be derived in an analogous manner and will be omitted here. The above equations indicate that the model and the truncation errors can be predicted or bounded if we either know or can reliably estimate or bound the channel dynamic. To evaluate the phase reconstruction error, we need to know the statistic of the reconstructed phases, which can be expressed as

$$\begin{aligned}\tilde{\theta}(k) &= \sum_{i=1}^{k} \cos^{-1}\left[\frac{I(i)I(i-1)+Q(i)Q(i-1)}{\sqrt{I^2(i)+Q^2(i)}\sqrt{I^2(i-1)+Q^2(i-1)}}\right] \\ &= \sum_{i=1}^{k}\left[\tan^{-1}\left(\frac{Q(i)}{I(i)}\right)-\tan^{-1}\left(\frac{Q(i-1)}{I(i-1)}\right)\right] \\ &= \tan^{-1}\left(\frac{Q(k)}{I(k)}\right)-\tan^{-1}\left(\frac{Q(0)}{I(0)}\right) \end{aligned} \tag{26}$$

where we have assumed, without loss of generality, that $\tan^{-1}[Q(0)/I(0)] = 0$. Note that these three equations are only mathematically equivalent; the limit range of a single arctan function forces us to use the first equation for phase reconstruction. Nevertheless, the last equation tells us that the phase reconstruction error is equal to the variance of $\theta = \tan^{-1}(Q(k)/I(k))$, whose probability density function (pdf) is given by [29]

$$\begin{aligned} f(\theta) = &\frac{e^{-\mu^2/2}}{2\pi} + \frac{\mu\cos(\theta-\psi)}{\sqrt{2\pi}} \\ &\cdot \exp\left[-\frac{\mu^2\sin^2(\theta-\psi)}{2}\right]\Phi[\mu\cos(\theta-\psi)] \end{aligned} \tag{27}$$

where ψ is the true phase, $\mu = \sqrt{P_r T_S/N_0}$, P_r is the received signal power, N_0 is one-sided power spectral density of the thermal noise, and the Φ function is defined as

$$\Phi(x) = \frac{1}{\sqrt{2\pi}}\int_{-\infty}^{x} e^{-y^2/2}\,dy. \tag{28}$$

There are two other effects that must be accounted for in evaluating the phase reconstruction error if we consider a digital implementation, namely, the analog-to-digital (A/D) conversion error and the quantization error. The former resulted from converting the samples $\{I(k), Q(k)\}$ to finite-bit numbers, and the latter is due to the fact that only finite-precision arctan values can be stored in a ROM. The conversion error depends on the A/D converter used, and the combined MSE analysis is well documented [3], assuming that a noncoherent AGC is in place. Hence we will omit further discussion on these two errors.

It is clear from the above analysis that the MSE is determined by the update speed T_F, the signal-to-noise ratio μ^2, the sample size N, the sampling rate $1/T_S$, and the channel dynamic (which directly affect the model and the truncation errors). Comparing (20) and (25), we find that the MS Doppler prediction errors for both the first- and second-order algorithms are of the same order. Equation (6), on the other hand, reveals that the MSE for the Doppler rate estimator is proportional to T_S^{-4}. Therefore, the optimal T_S associated with each algorithm is different, but the concern of the Doppler rate estimator's reliability often forces us to use a larger T_S for the second-order algorithm.

We next extend our investigation to an uncorrelated Rician fading environment characterized by the following received signal model [30]:

$$I(k) = (\alpha+u_1)\cos(\Delta\theta_k) + u_2\sin(\Delta\theta_k) + n_I(k) \tag{29}$$

$$Q(k) = (\alpha+u_1)\sin(\Delta\theta_k) - u_2\cos(\Delta\theta_k) + n_Q(k) \tag{30}$$

where u_1 and u_2 are independent zero-mean Gaussian random variables with a common variance N_u. It is shown in the Appendix that the pdf of $\tilde{\theta}(k)$ for this case is the same as (27) except that $\mu = \sqrt{P_r T_S/(N_0+N_u)}$.

The third case to be considered is the correlated Rician fading channel under which the diffuse components u_1, u_2 of the received signal become independent first-order Gauss–Markov processes

$$u_1(k+1) = \rho u_1(k) + v_1(k) \tag{31}$$

$$u_2(k+1) = \rho u_2(k) + v_2(k) \tag{32}$$

where $\{v_1(k)\}$ and $\{v_2(k)\}$ are independent white Gaussian sequences with the variance $(1-\rho^2)\sigma_u^2$. The resulting MSE can be obtained by replacing the first terms on the right-hand side of (18) and (23) by

$$\begin{aligned} &E\left[\left(\lambda_N\sum_{k=1}^{N}(2k-N-1)\epsilon_{r_1}(k)\right)^2\right] \\ &\quad = \lambda_N^2\sum_{l=1-N}^{N-1}\sum_{k=1}^{N}(2k-N-1)[2(k-l)-N-1]\sigma_{\epsilon_{r_1}}^2(l) \end{aligned} \tag{33}$$

and

$$\begin{aligned} &E\left\{\left(\frac{\alpha_N}{T_S}\sum_{k=1}^{N}[\beta_N(k-N-1)/15+(2N+1)\gamma_N/10\right.\right. \\ &\qquad +(N+1)(k-N-1)^2]\epsilon_{r_2}(k)+\frac{2\alpha_N}{T_S^2}(t_f-t_{N+1}) \\ &\qquad \left.\left.\cdot\sum_{k=1}^{N}[k^2-(N+1)k+\gamma_N/6]\epsilon_{r_2}(k)\right)^2\right\} \\ &= \frac{\alpha_N^2}{T_S^2}\sum_{l=1-N}^{N-1}\sum_{k=1}^{N}[\beta_N(k-N-1)/15+(2N+1) \\ &\quad \cdot\gamma_N/10+(N+1)(k-N-1)^2] \\ &\quad \times[\beta_N(k-l-N-1)/15+(2N+1)\gamma_N/10 \\ &\qquad +(N+1)(k-l-N-1)^2]\sigma_{\epsilon_{r_2}}^2(l) \\ &\quad +\frac{4\alpha_N^2}{T_S^4}(t_f-t_{N+1})^2\sum_{l=1-N}^{N-1}\sum_{k=1}^{N}[k^2-(N+1)k+\gamma_N/6] \\ &\quad \times[(k-l)^2-(N+1)(k-l)+\gamma_N/6]\sigma_{\epsilon_{r_2}}^2(l) \\ &\quad -\frac{2\alpha_N^2}{T_S^3}(t_f-t_{N+1})\sum_{l=1-N}^{N-1}\sum_{k=1}^{N}[\beta_N(k-N-1)/15 \\ &\qquad +(2N+1)\gamma_N/10+(N+1)(k-N-1)^2] \\ &\quad \times[(k-l)^2-(N+1)(k-l)+\gamma_N/6]\sigma_{\epsilon_{r_2}}^2(l) \end{aligned} \tag{34}$$

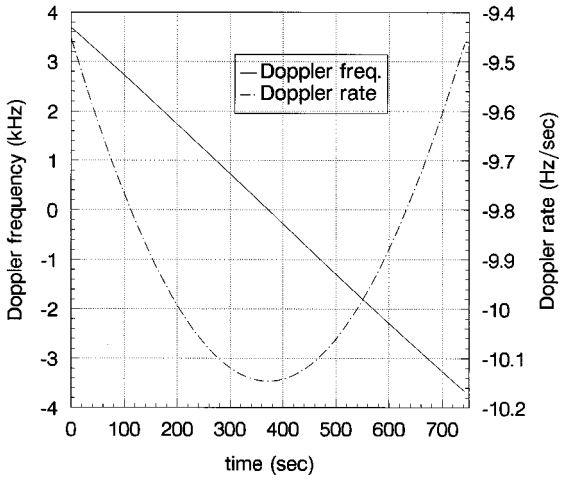

Fig. 3. Doppler frequency and Doppler rate at ground terminal; LEO satellite altitude is 7000 km; transmitted signal frequency is 1.5 GHz.

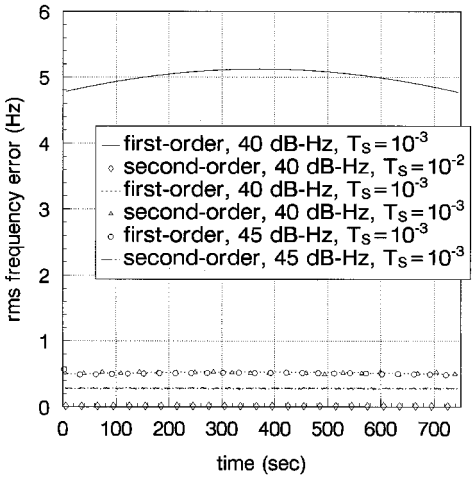

Fig. 4. RMS frequency tracking error at T_1; $T_F = 1$ s.

where $\sigma^2_{\epsilon_{r_i}}(l)$ is the covariance between two reconstructed phases θ_1, θ_2 separated by l sampling intervals and can be computed from their joint pdf derived in the Appendix.

IV. Numerical Examples

To investigate the numerical behaviors of the proposed algorithms, computer simulations were conducted. For most of the simulation results reported here, the channel dynamic of Fig. 3, which represents the time span for a satellite at 7000 km altitude to move from 73° to 107° of elevation angle, is assumed. The number of samples for each batch N is chosen to be 100 and $T_F = 1$ s. The time right after the nth update is denoted by T_1, i.e., $T_1 = nT_F + T_S$, for some $n \geq 1$; the time in the middle of two adjacent updates is denoted by T_2; and $T_3 = nT_F + NT_S$ is the time right before a new update is to be output.

As shown in Fig. 4, the root mean square (rms) frequency prediction error of the second-order LS algorithm at T_1 is superior to that of the first-order algorithm if the sampling rate $1/T_S$ is chosen appropriately. For a fixed sampling rate, the rms frequency error is a decreasing function of the CNR. Fig. 5 shows the rms frequency tracking errors at T_2 and T_3, respectively.

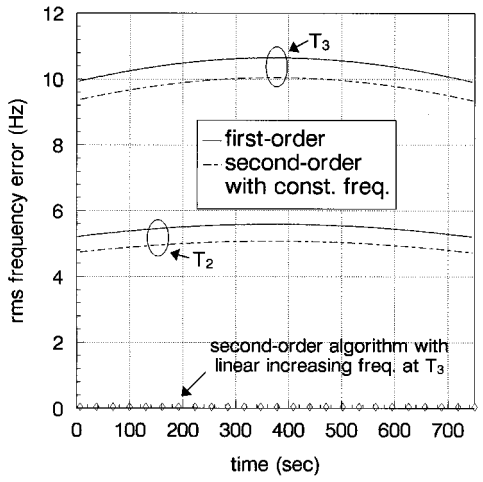

Fig. 5. RMS frequency tracking errors at T_2 and T_3, CNR $= 40$ dB-Hz.

The sampling interval for the first-order algorithm is 10^{-3} s, while that for the second-order algorithm is 10^{-2} s as the numerical results presented in Fig. 4 indicate these are the better choices for them. Also shown in Fig. 5 is the performance of another second-order algorithm, which, instead of a constant forward-predicting frequency signal, causes the NCO to generate a local CW signal with linearly increased frequency, i.e., during a T_F sinterval, the NCO output signal has a phase that is governed by (5b) where t_i is the time elapsed since the last update $\{\hat{\omega}_D, \hat{\dot{\omega}}_D\}$ is given. We did not provide the performance of this algorithm in Fig. 4 because it is indistinguishable from that of the other second-order algorithm at $t = T_1$. The latter algorithm becomes inferior to the former algorithm when we compare their performance at T_2 and T_3 because it has larger model and truncation errors.

Rician fading is often parameterized by $\gamma^2 = \alpha^2/\sigma_u^2$, the ratio of the energy in the specular component to the average energy in the diffuse component. Fig. 6 compares the performance in AWGN and Rician fading channels with various correlation coefficient ρ, where $\overline{\text{CNR}}$ denotes the average CNR. In all cases, the second-order LS algorithm always outperforms the first-order algorithm. The relationship between $\sigma^2_{\Delta\omega}$ and ρ is clearly not linear. The MSE of the first-order algorithm, as (33) indicates, can be decomposed into two parts

$$2\sum_{k=1}^{N/2}\sum_{l=1}^{N/2}(2k-N-1)(2l-N-1)\sigma^2_{\epsilon_{r_1}}(k-l) + 2\sum_{k=(N/2)+1}^{N}\sum_{l=1}^{N/2}(2k-N-1)(2l-N-1)\sigma^2_{\epsilon_{r_1}}(k-l) \tag{35}$$

where the first term is positive and the second term is negative. Since the covariance $\sigma^2_{\epsilon_{r_1}}(l)$ increases as ρ increases or l decreases, the MSE rate of change at a particular ρ depends on the covariance's rate of change with respect to ρ and l. There seems to be no general rule to predict the MSE behavior as a function of channel correlation coefficient.

The MSE caused by the modeling and the truncation errors is deterministic if the transmitter trajectory and the algorithm

TABLE II
MEAN SQUARED FREQUENCY TRACKING ERROR PREDICTED BY ANALYSIS AND SIMULATION

	40 dB-Hz		45 dB-Hz	
first-order	analysis	simulation	analysis	simulation
AWGN, $T_S = 10^{-3}$	1.61×10^{-2}	1.5997×10^{-2}	4.886×10^{-3}	4.967×10^{-3}
AWGN, $T_S = 10^{-2}$	1.53×10^{-5}	1.535×10^{-5}	4.8×10^{-6}	4.755×10^{-6}
Rician, $\rho = 0$, $\gamma = 4$, $T_S = 10^{-3}$	4.353×10^{-2}	4.016×10^{-2}	2.716×10^{-2}	2.705×10^{-2}
second-order				
AWGN, $T_S = 10^{-3}$	0.26254	0.2624	7.968×10^{-2}	7.93×10^{-2}
AWGN, $T_S = 10^{-2}$	2.49×10^{-4}	2.489×10^{-4}	7.85×10^{-5}	7.817×10^{-5}
Rician, $\rho = 0$, $\gamma = 4$, $T_S = 10^{-2}$	3.677×10^{-3}	3.665×10^{-3}	3.4478×10^{-3}	3.437×10^{-3}

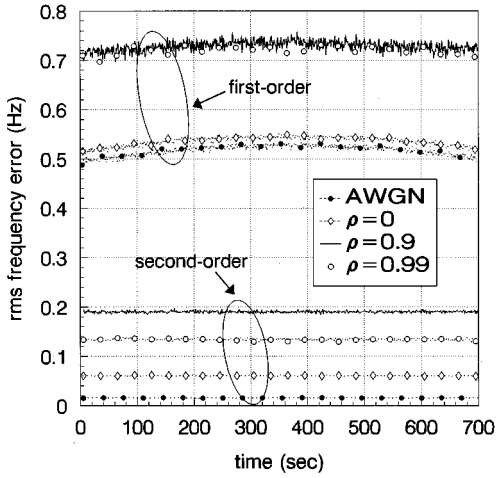

Fig. 6. Performance of the LS frequency tracking algorithm over Rician fading channels at T_1, $\gamma = 4$; $\overline{\text{CNR}} = 40$ dB-Hz.

used are known. Furthermore, this part of MSE is independent of the other part caused by the phase reconstruction error. Therefore, the sample mean of $\omega_D - \hat{\omega}_D$ derived from simulation represents the frequency error due to the former two errors, and the sample variance is the MSE caused by the latter error only. Table II lists the mean squared frequency tracking error induced by the phase reconstruction error predicted, respectively, by our analysis and by simulations. These numbers reveal that our analysis does yield very reliable estimation for the MS frequency tracking error.

The performance of the recursive form is the same as that of the batch form at T_1. The superiority of the second-order algorithm is made clearer in Fig. 7, where we compare the performance of both algorithms listed in Table I(a) and (b) for a higher dynamic environment as that given by Fig. 1. Natali [1] presented eight different AFC loop configurations and compared their performance. His simulation indicates that the cross-product AFC and its analog version yield the best performance for CW and differential phase-shift keying signals, although their advantage is not too impressive; see [1, Figs. 20 and 21]. Cahn [2] has suggested the use of a third-order digital cross-product AFC loop to combat high channel dynamics. This digital loop is implemented by discretizing a second-order Jaffe–Rechtin filter with bandwidth B_L

$$e(k) = Q(k)I(k-1) - I(k)Q(k-1) \tag{36}$$

$$\hat{\dot{\omega}}(k+1) = \hat{\dot{\omega}}(k) + \gamma e(k) \tag{37}$$

$$\hat{\omega}(k+1) = \hat{\omega}(k) + T_F\hat{\dot{\omega}}(k) + \sqrt{2}\gamma e(k) \tag{38}$$

$$\hat{\theta}(k+1) = \hat{\theta}(k) + T_F\hat{\omega}(k) \tag{39}$$

where $\gamma = 1.89B_L$ and T_F is the update (sampling) period. For $B_L T_F \ll 1$, the rms frequency tracking error is [2] $\sigma_{\Delta\omega} = B_L^{0.5} T_F^{-1.5}(N_0/S)$. Fig. 7 also depicts the rms frequency error trajectories in AWGN and uncorrelated Rician channels for the above AFC loop with $\overline{\text{CNR}} = 50$ dB-Hz, $B_L = 10$ Hz, and a update period $T_F = 10^{-5}$ ss. We can clearly see that the steady-state rms frequency tracking error for the AFC loop is much larger than that of the LS algorithms. The transient behavior of the loop is not shown for fear of masking the difference in steady-state performance. It takes the AFC loop about 0.6 s to reach the steady state (from an initial Doppler offset of 35 kHz). In contrast, our algorithms need only 1 ms (100 samples with a sampling rate $= 10^5$ samples/s) to produce the initial frequency estimate whose rms error is negligible when compared with that of the third-order AFC loop. We have to stress that better AFC performance might still be obtained by exploiting error signals other than those discussed in [1].

V. CONCLUSIONS

We have presented MSE analysis of two classes of frequency acquisition and tracking algorithms for use in high dynamic environments. Both batch form and recursive form are suitable for real-time implementation. The class of batch form algorithms is a simple extension of existing algorithms, but the recursive algorithms need major modifications. These algorithms are of low complexity and have fast acquisition time and low tracking jitter. They can also be modified to track the frequency of a phase-modulated signal if a nonlinear preprocessor to remove data modulation is added or a timing-directed phase unwrapping methods is in place.

Unlike previous similar MSE analyses that use Gaussian assumptions, our analysis uses the exact reconstructed phase distributions. Simulation results showed that our MSE estimation is quite accurate. Furthermore, the resulting performance is far superior to that of a third-order cross product AFC loop. The effects of various design parameters—sampling rate, sample or window size, order of signal phase trajectory approximation—and system and channel dynamic parameters—CNR, maximum Doppler, and Doppler rate—can be deduced from our MSE analysis. It also enables us to study performance and design parameter tradeoffs. Although we concentrated our effort on the first- and second-order algorithms, the concept and the analysis can easily be extended to higher order algorithms if needed.

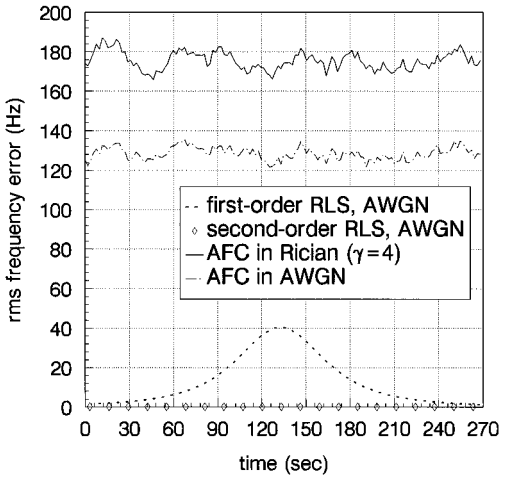

Fig. 7. Recursive least squares (RLS) frequency-tracking algorithms and steady-state behavior of Cahn's third-order AFC loop at $\overline{\text{CNR}} = 50$ dB-Hz. The transient behavior ($0 \sim 0.6$ s) of the AFC loop is not shown.

APPENDIX
RECONSTRUCTED PHASE DISTRIBUTIONS IN RICIAN FADING CHANNELS

The received signal can be decomposed as

$$\begin{aligned} I &= [\alpha \cos\psi + u_1 \cos\psi + u_2 \sin\psi] + n_I = I' + n_I \\ Q &= [\alpha \sin\psi + u_1 \sin\psi - u_2 \cos\psi] + n_Q = Q' + n_Q \end{aligned} \tag{A.1}$$

where n_I and n_Q are independent Gaussian random variables with variance σ_n^2. Using the change of variables

$$I = R\cos\theta, \quad Q = R\sin\theta$$

we obtain the conditional joint pdf of R and θ given u_1 and u_2

$$\begin{aligned} f(R, \theta | u_1, u_2) = {} & \frac{R}{2\pi\sigma_n^2} \exp\left[-\frac{R^2 + \alpha^2 - 2\alpha R\cos(\theta - \psi)}{2\sigma_n^2}\right] \\ & \cdot \exp\left[-\frac{u_1^2 - 2R\cos(\theta - \psi)u_1 + 2\alpha u_1}{2\sigma_n^2}\right] \\ & \cdot \exp\left[-\frac{u_2^2 + 2R\sin(\theta - \psi)u_2}{2\sigma_n^2}\right] \end{aligned} \tag{A.2}$$

where $0 \le R < \infty$ and $0 \le \theta \le 2\pi$. The unconditional joint pdf of R and θ is given by

$$f(R, \theta) = \int_{-\infty}^{\infty}\int_{-\infty}^{\infty} f(R, \theta | u_1, u_2) f(u_1) f(u_2)\, du_1\, du_2 \tag{A.3}$$

where $f(u_1)$, $f(u_2)$ are the density function of u_1, u_2. The fact that u_1 and u_2 are i.i.d. Gaussian random variables with variance σ_u^2 leads to

$$\begin{aligned} & \int_{-\infty}^{\infty} \frac{1}{\sigma_u\sqrt{2\pi}} \exp\left(-\frac{u_1^2}{2\sigma_u^2}\right) \\ & \quad \cdot \exp\left[-\frac{u_1^2 - 2R\cos(\theta - \psi)u_1 + 2\alpha u_1}{2\sigma_n^2}\right] du_1 \\ & = \frac{\sigma_n}{\sqrt{\sigma_n^2 + \sigma_u^2}} \exp\left\{\frac{\sigma_u^2[\alpha - R\cos(\theta - \psi)]^2}{2\sigma_n^2(\sigma_n^2 + \sigma_u^2)}\right\} \end{aligned} \tag{A.4}$$

and

$$\begin{aligned} & \int_{-\infty}^{\infty} \frac{1}{\sigma_u\sqrt{2\pi}} \exp\left(-\frac{u_2^2}{2\sigma_u^2}\right) \\ & \quad \cdot \exp\left[-\frac{u_2^2 + 2R\sin(\theta - \psi)u_2}{2\sigma_n^2}\right] du_2 \\ & = \frac{\sigma_n}{\sqrt{\sigma_n^2 + \sigma_u^2}} \exp\left\{\frac{[\sigma_u R\sin(\theta - \psi)]^2}{2\sigma_n^2(\sigma_n^2 + \sigma_u^2)}\right\}. \end{aligned} \tag{A.5}$$

By substituting (A.4) and (A.5) into (A.3), we obtain

$$\begin{aligned} f(R, \theta) = {} & \frac{R}{2\pi(\sigma_n^2 + \sigma_u^2)} \exp \\ & \cdot \left[-\frac{R^2 + \alpha^2 - 2\alpha R\cos(\theta - \psi)}{2(\sigma_n^2 + \sigma_u^2)}\right] \end{aligned} \tag{A.6}$$

and the marginal pdf of θ

$$\begin{aligned} f(\theta) &= \int_0^{\infty} f(R, \theta)\, dR \\ &= \frac{e^{-\mu^2/2}}{2\pi} + \frac{\mu\cos(\theta - \psi)}{\sqrt{2\pi}} \\ &\quad \cdot \exp\left[-\frac{\mu^2\sin^2(\theta - \psi)}{2}\right] \Phi[\mu\cos(\theta - \psi)] \end{aligned} \tag{A.7}$$

where $\mu = \alpha/\sqrt{\sigma_n^2 + \sigma_u^2}$. Comparing the above equation with (A.1), we conclude that an equivalent model for the received I and Q samples is

$$\begin{aligned} I &= \alpha\cos\psi + n_I' \\ Q &= \alpha\sin\psi + n_Q' \end{aligned} \tag{A.8}$$

where n_I' and n_Q' are i.i.d. zero-mean Gaussian random variables with variance $\sigma_n^2 + \sigma_u^2$.

Next let us consider the case when the diffuse components n_I', n_Q' at different times are correlated and can be modeled as independent Gauss–Markov processes. Denote the random variables $I(k)$, $Q(k)$, $I(k-l)$, $Q(k-l)$ by

$$\boldsymbol{X} = [I(k), Q(k), I(k-l), Q(k-l)]^t. \tag{A.9}$$

The corresponding mean vector $\boldsymbol{\mu}$ is

$$E[\boldsymbol{X}] = \boldsymbol{\mu} = [\alpha\cos\psi_1, \alpha\sin\psi_1, \alpha\cos\psi_2, \alpha\sin\psi_2]^t \tag{A.10}$$

and the joint probability density function is given by

$$\begin{aligned} f(\boldsymbol{X}) = {} & (2\pi\sigma_u^2)^{-2}|\boldsymbol{P}|^{-1/2} \\ & \cdot \exp\left[\frac{-1}{2\sigma_u^2}(\boldsymbol{X} - \boldsymbol{\mu})'\boldsymbol{P}^{-1}(\boldsymbol{X} - \boldsymbol{\mu})\right] \end{aligned} \tag{A.11}$$

where

$$\boldsymbol{P} = \begin{bmatrix} a & 0 & \rho^l & 0 \\ 0 & a & 0 & \rho^l \\ \rho^l & 0 & a & 0 \\ 0 & \rho^l & 0 & a \end{bmatrix} \tag{A.12}$$

is the covariance matrix with $a = 1 + \sigma_n^2/\sigma_u^2$ and

$$|\boldsymbol{P}|^{-1/2} = (a^2 - \rho^{2l})^{-1} \tag{A.13}$$

$$\boldsymbol{P}^{-1} = \frac{1}{a^2-\rho^{2l}} \begin{bmatrix} a & 0 & -\rho^l & 0 \\ 0 & a & 0 & -\rho^l \\ -\rho^l & 0 & a & 0 \\ 0 & -\rho^l & 0 & a \end{bmatrix} \equiv \frac{1}{a^2-\rho^{2l}} \boldsymbol{P_1}. \quad \text{(A.14)}$$

After the changes of variables, $I(k) = R_1 \cos\theta_1$, $Q(k) = R_1 \sin\theta_1$, $I(k-l) = R_2 \cos\theta_2$, $Q(k-l) = R_2 \sin\theta_2$, and some algebraic manipulation, we obtain

$$\begin{aligned} f(R_1, R_2, \theta_1, \theta_2) &= c \cdot R_1 R_2 \\ &\cdot \exp\left(\frac{-1}{2\sigma_u^2(a^2-\rho^{2l})} \right. \\ &\cdot \{a[R_1^2 + R_2^2 - 2\alpha R_1 \cos(\theta_1 - \psi_1) \\ &- 2\alpha R_2 \cos(\theta_2 - \psi_2)] \\ &- 2\rho^l [R_1 R_2 \cos(\theta_1 - \theta_2) - \alpha R_1 \cos(\theta_1 - \psi_2) \\ &\left. -\alpha R_2 \cos(\theta_2 - \psi_1)]\} \right) \end{aligned} \quad \text{(A.15)}$$

with

$$\begin{aligned} c &= (2\pi\sigma_u^2)^{-2}(a^2-\rho^{2l})^{-1} \\ &\cdot \exp\left\{ \frac{-1}{\sigma_u^2(a^2-\rho^{2l})} \alpha^2 [a - \rho^l \cos(\psi_1 - \psi_2)] \right\}. \end{aligned} \quad \text{(A.16)}$$

The integration

$$f(\theta_1, \theta_2) = \int_0^\infty \int_0^\infty f(R_1, R_2, \theta_1, \theta_2)\, dR_1\, dR_2 \quad \text{(A.17)}$$

then leads to

$$\begin{aligned} f(\theta_1, \theta_2) &= c \int_0^\infty R_2 \exp\{-[aR_2^2 - 2a\alpha R_2 \cos(\theta_2 - \psi_2) \\ &+ 2\alpha R_2 \rho^l \cos(\theta_2 - \psi_1) - q^2/a]/2\sigma_u^2(a^2-\rho^{2l})\} \\ &\times \frac{1}{a} \left\{ \sigma_u^2(a^2-\rho^{2l}) \exp\left[\frac{-q^2/(2a\sigma_u^2)}{(a^2-\rho^{2l})} \right] \right. \\ &\left. + \frac{q}{\sqrt{a}} \sigma_u \sqrt{2\pi(a^2-\rho^{2l})} \Phi\left(\frac{q/(\sigma_u\sqrt{a})}{\sqrt{a^2-\rho^{2l}}} \right) \right\} dR_2 \end{aligned} \quad \text{(A.18)}$$

where c is defined by (A.16) and q is a function of R_2, θ_1, and θ_2; more specifically

$$\begin{aligned} q &= \alpha \cos(\theta_1 - \psi_1) - \alpha\rho^l \cos(\theta_1 - \psi_2) \\ &+ R_2 \rho^l \cos(\theta_1 - \theta_2). \end{aligned} \quad \text{(A.19)}$$

REFERENCES

[1] A. F. Natali, "AFC tracking algorithms," *IEEE Trans. Commun.*, vol. COM-32, pp. 935–947, Aug. 1984.

[2] C. R. Cahn, D. K. Leimer, and C. L. Marsh, "Software implementation of a PN spread spectrum receiver to accommodate dynamics," *IEEE Trans. Commun.*, vol. COM-25, pp. 832–840, Aug. 1977.

[3] Y. T. Su and H. J. Choi, "Noncoherent sampling technique for communications parameter estimations," in *Proc. Int. Telemetering Conf.*, Oct. 1985, pp. 301–308.

[4] S. Bellini, C. Molinari, and G. Tartara, "Digital frequency estimation in burst mode QPSK transmission," *IEEE Trans. Commun.*, vol. 38, pp. 959–961, July 1990.

[5] S. A. Tretter, "Estimating the frequency of a noisy sinusoid by linear regression," *IEEE Trans. Inform. Theory*, vol. IT-31, pp. 832–835, Nov. 1985.

[6] S. Aguirre and S. Hinedi, "Two novel automatic frequency tracking loops," *IEEE Trans. Aerosp. Electron. Syst.*, vol. 25, pp. 749–760, Sept. 1989.

[7] D. C. Rife and R. R. Boorstyn, "Single-tone parameter estimation from discrete-time observations," *IEEE Trans. Inform. Theory*, vol. IT-20, pp. 591–598, Sept. 1974.

[8] T. J. Abatzoglou, "A fast maximum likelihood algorithm for frequency estimation of a sinusoid based on Newton's method," *IEEE Trans. Acoust., Speech, Signal Proc.*, vol. ASSP-33, pp. 77–89, Feb. 1985.

[9] ——, "Fast maximum likelihood joint estimation of frequency and frequency rate," *IEEE Trans. Aerosp. Electron. Syst.*, vol. AES-22, pp. 708–715, Nov. 1986.

[10] W. J. Hurd, J. I. Statman, and V. A. Vilnrotter, "High dynamic GPS receiver using maximum likelihood estimation and frequency tracking," *IEEE Trans. Aerosp. Electron. Syst.*, vol. AES-23, pp. 425–436, July 1987.

[11] J. C.-I. Chuang, "Burst coherent demodulation with combined symbol timing, frequency offset estimation, and diversity selection," *IEEE Trans. Commun.*, vol. 39, pp. 1157–1164, July 1991.

[12] R. Kumar, "Frequency estimation techniques for high dynamic trajectories," *IEEE Trans. Aerosp. Electron. Syst.*, vol. 25, no. 4, pp. 559–577, July 1989.

[13] ——, "A novel multistage estimation of signal parameters," *IEEE Trans. Aerosp. Electron. Syst.*, vol. 26, pp. 181–194, Jan. 1990.

[14] S. Kay, "A fast and accurate single frequency estimator," *IEEE Trans. Acoust., Speech, Signal Processing*, vol. 37, pp. 1987–1990, Dec. 1989.

[15] P. M. Djuric and S. M. Kay, "Parameter estimation of chirp signals," *IEEE Trans. Acoust., Speech, Signal Processing*, vol. 38, pp. 2118–2126, Dec. 1990.

[16] S. W. Lang and B. R. Musicus, "Frequency estimation from phase differences," *Proc. Int. Conf. Acoustics, Speech and Signal Processing*, pp. 2140–2144, 1989.

[17] S. H. Knowles and W. B. Waltman, "Linear least-squares determination of Doppler time derivative for NAVSPASUR-like signals," *IEEE Trans. Instrum. Meas.*, vol. IM-34, pp. 64–69, Mar. 1985.

[18] M. McIntyre and A. Ashley, "A simple fixed-lag algorithm for tracking frequency rate-of-change," *IEEE Trans. Aerosp. Electron. Syst.*, vol. 29, pp. 677–683, July 1993.

[19] A. J. Viterbi and A. M. Viterbi, "Nonlinear estimation of PSK-modulated carrier phase with application to burst digital transmission," *IEEE Trans. Info. Theory*, vol. IT-29, pp. 543–550, July 1983.

[20] M. K. Simon and D. Divsalar, "Doppler-corrected differential detection of MPSK," *IEEE Trans. Commun.*, vol. 37, pp. 99–109, Feb. 1989.

[21] M. P. Fitz and W. C. Lindsey, "Decision-directed burst-mode carrier synchronization techniques," *IEEE Trans. Commun.*, vol. 40, pp. 1644–1653, Oct. 1992.

[22] M. P. Fitz, "Planar filtered techniques for burst mode carrier synchronization," in *IEEE Global Telecommun. Conf.*, Phoenix, AZ, Dec. 1991, pp. 365–369.

[23] F. Classen, H. Meyr, and P. Sehier, "Maximum likelihood open loop carrier synchronizer for digital radio," in *Proc. IEEE Int. Conf. Commun.*, vol. 1, Geneva, 1993, pp. 493–497.

[24] U. Mengali and M. Morelli, "Data-aided frequency estimation for burst digital transmission," *IEEE Trans. Commun.*, vol. 45, pp. 23–25, July 1997.

[25] M. Luise and R. Reggiannini, "Carrier frequency recovery in all-digital modems for burst-mode transmissions," *IEEE Trans. Commun.*, vol. 43, pp. 1169–1178, Feb/Mar./Apr. 1995.

[26] J. M. Tribolet, *Seismic Applications of Homomorphic Signal Processing*: Prentice Hall, 1979.

[27] F. Classen and H. Meyr, "Two frequency estimation schemes operating independently of timing information," in *Proc. IEEE Global Telecommun. Conf.* Houston, TX, Nov.–Dec. 1993, vol. 3, pp. 1996–2000.

[28] A. N. D'Andrea, A. Ginesi, and U. Mengali, "Digital carrier frequency estimation for multilevel CPM signal," in *Proc. IEEE Int. Conf. Commun.*, vol. 2, Seattle, WA, June 1995, pp. 1041–1045.

[29] J. B. Thomas, *An Introduction to Statistical Communication Theory*. Englewood Cliffs, NJ: Prentice-Hall, 1962.

[30] H. L. Van Trees, *Detection, Estimation, and Modulation Theory*. New York: Wiley, 1968, vol. 1, pp. 360–364.

Yu T. Su received the Ph.D. degree from the University of Southern California, Los Angeles, in 1983.

From 1983 to 1989, he was with LinCom Corporation, Los Angeles, CA, where he was involved in the design of digital satellite communication systems. Since September 1989, he has been with the Department of Communication Engineering and the Microelectronics and Information Systems Research Center, National Chiao Tung University, Hsinchu, Taiwan. His areas of research interest are communication theory and statistical signal processing.

Ru-Chwen Wu received the B.S., M.S., and Ph.D. degrees in electrical engineering from the Department of Communication Engineering, National Chiao Tung University, Hsinchu, Taiwan, in 1991, 1993, and 2000, respectively.

Since 1999, she has been with the Computer Communication Laboratory, Industrial Technology Research Institute, Hsinchu, Taiwan. Her main research interests include spread-spectrum communications and synchronization theory.